Proceedings of the 10th International Conference on Fluid Flow, Heat and Mass Transfer (FFHMT'23)
Ottawa, Canada – June 07-09, 2023
Paper No. 173
DOI: 10.11159/ffhmt23.173

Effects of Geometrical Parameters on Thermal-Hydraulic performance of air flowing in Additively Manufacturable Heat Exchanger

C. Chaitanya Kishore[1], V. Raghavan[2], G. Venkatarathnam[2]
[1,2]Department of Mechanical Engineering
IIT Madras, Chennai-600036, India
me20s026@smail.iitm.ac.in; raghavan@iitm.ac.in
gvenkat@iitm.ac.in

Abstract **-** An additively manufactured airfoil finned plate-fin heat exchanger (PFHE) is proposed to be applied to a flue gas waste heat recovery system. This study numerically investigates the effect of various geometrical characteristics of the airfoil finned channel on the pressure drop and heat transfer using OpenFOAM with dry air as a working cold fluid. The studied parameters include the offset number (ξ_f), longitudinal number (ξ_l), transverse number (ξ_t), and fin height (h_f) of the airfoil. Additionally, the effect of the fin number on the thermal-hydraulic characteristics of the flow channel is also studied to determine the minimum number of fins where the friction factor and Colburn j-factor variation along the flow length is nearly stabilized. The results of the study show that the 20 number of fins is reasonable for assessing the heat exchanger performance. The offset number has an influence on pressure drop and heat transfer until the offset length approaches the fin length, after which it has no effect. The longitudinal number effect on heat transfer per unit area and pressure drop per unit length is a linear variation, while the transverse number and fin height effect is a non-linear variation.

Keywords**:** Airfoil fin, CFD, Additive manufacturing, Heat exchanger, Flue gas waste heat recovery, Pressure drop

1. Introduction

In recent years, the energy demand in various industries has increased rapidly. With limited fossil fuel reserves and abundant waste heat resources, waste heat recovery stands as an alternate energy source, reducing reliance on fossil fuels. In power plants and other industrial processes, waste heat recovery from high-temperature exhaust flue gas can significantly improve energy utilisation efficiency, cost savings, and environmental impact. Therefore, many scholars conducted extensive research on flue gas heat exchangers, one of the key equipments in waste heat recovery systems.

Plate-fin heat exchangers (PFHE) use fins or extended surfaces to increase the heat transfer surface area density. Fins in PFHEs also increase thermal effectiveness by disrupting the boundary layer formation [1]. Some conventional fin structures used in industrial PFHEs include offset-strip fins, wavy fins, louvered fins, perforated fins, and serrated fins [2]. However, recent advancements in manufacturing technologies like additive manufacturing (AM) have enabled the development of heat exchangers with much more complex fin surfaces and greater geometric freedom driven by flow requirements. These innovations offer the potential for increased heat transfer efficiency and improved energy conservation in various industrial applications.

Some of the unconventional fins used in heat transfer devices are mentioned here. Unger et al. [3], [4] developed novel serrated integrated pin fin (SIPF) and circular integrated pin fin (CIPF) using AM. Effects of tube tilt angle, and tube row number on thermal-hydraulic characteristics were extensively studied on these fins. A novel AM heat exchanger was fabricated by Gestler et al. [5] to meet the heat transfer and fluid pressure drop requirements of an oil cooler. The mass and volume of the AM heat exchanger were 66 and 50 percent lower than the baseline oil cooler at similar performance. Wong et al. [6] investigated on elliptical fin heat sinks and concluded that elliptical fin heat sinks have the highest heat transfer per unit pressure drop compared to pin fin heat sinks. Pracht et al. [7] studied experimentally and numerically a 3D-printed modified rhombus-shaped finned aluminum cryogenic heat exchanger for compact Brayton Refrigerators. Han et al. [8] investigated the thermal-hydraulic characteristics of printed circuit heat exchanger (PCHE) with novel airfoil fins, NACA0020 airfoil fins, and conventional zigzag fins and showed that the overall performance of airfoil fins is better than zigzag fins. Shi et al. [9] investigated the thermal–hydraulic characteristics of S-CO_2 and molten-salt in novel PCHE with

airfoil fins. Chen et al. [10] numerically investigated the thermal-hydraulic behaviour of an airfoil finned recuperator with humid air as a working fluid.

The review of literature shows that researchers have used streamlined bodies like ellipses and airfoil shapes as fins in AM heat sinks and PCHEs. For waste heat recovery from flue gas to air application, only Chen et al. [10] used a PCHE with airfoil fins and developed friction factor and Nusselt number correlations with airfoil fins for air as a working fluid. However, the effect of geometrical parameters of airfoil fins using air as a working fluid has not been thoroughly investigated. This study investigates the effect of fin height, fin arrangement, and fin spacing in longitudinal and transverse directions on thermal-hydraulic characteristics with dry air as a working fluid inside channels with airfoil fins of AM waste heat recovery heat exchanger.

2. Numerical Methodology

2.1. Computational Domain

The physical model of the heat exchanger is adapted from Chen's [10] study. Due to the periodic and symmetric nature of heat transfer channels in the heat exchanger, a straight fin channel and an airfoil fin channel are chosen as the simulation domain. The simulation regions are shown in Fig. 1, with NACA0020 airfoil fins on the air side and straight fins on the flue gas side. Salome 5.7.0 has been used to form the computational domains of the airfoil finned counterflow heat exchanger. The details of the geometrical dimensions of the simulation domain are listed in Table 1. The heat exchanger domain includes three regions: the dry air region, the flue gas region, and the solid region. The solid region includes the separating walls between two fluid regions, airfoil fins, and straight fins.

The boundary conditions for the simulation domain are shown in Fig. 1 and Fig. 2. The periodic boundary condition is applied for the bottom and top surfaces, and the symmetric boundary condition is applied for the left and right faces. A constant velocity with a temperature of 823 K is applied at the inlet of hot flue gas, and 383 K is applied at the inlet of cold dry air. A constant pressure outlet boundary condition is used at the outlet of both heat transfer fluids. The dry air mass flow rate is 90% of the flue gas mass flow rate [10].

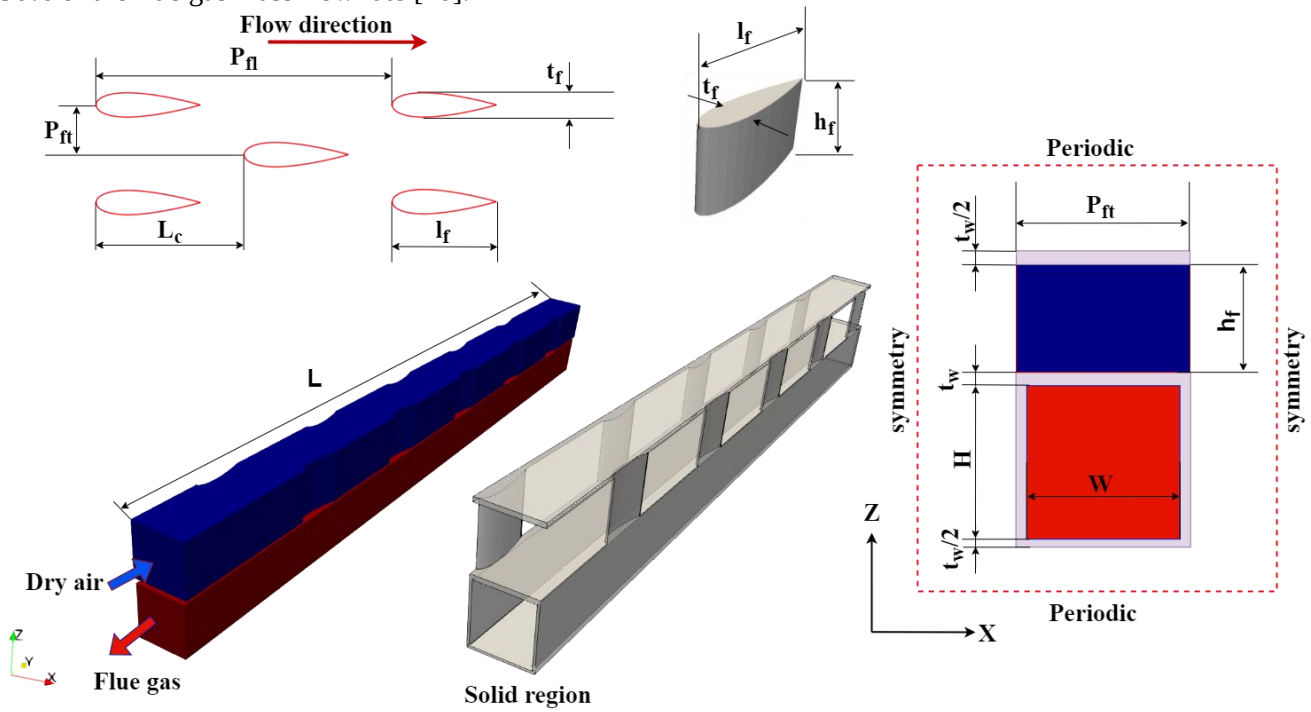

Fig. 1: Schematic diagram of the computational domain

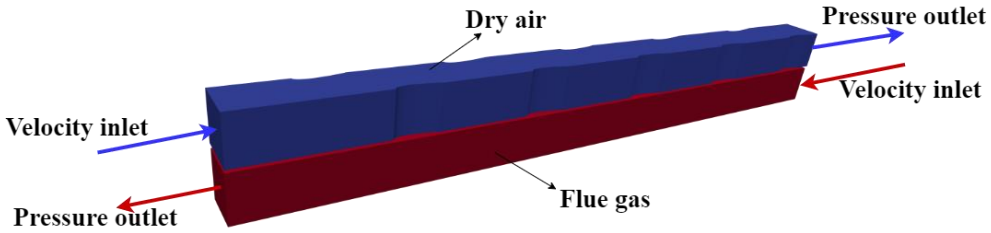

Fig. 2: Boundary conditions

Table 1: Dimensions of the simulation domain

Dimension	Size/mm	Dimension	Size/mm
Width W	3.7	Height of fin	h_f
Height of straight fin H	4	Longitudinal pitch	P_{fl}
Thickness of fin t_f	0.8	Transverse pitch	P_{ft}
Length of fin l_f	4	Fin Offset length	L_c
Thickness of wall t_w	0.3	Fin number	N

2.2. Properties of fluids and solid region

From Chen et al. [10], the hot fluid is normal pressure flue gas, and the cold fluid is 0.7 MPa dry air. The flue gas composition in volume fraction is H_2O 5.2 %, CO_2 3.04 %, O_2 16.09 %, and N_2 75.6 %, corresponding to dry air. REFPROP is used to calculate the properties of dry air. Table 2 displays the properties of the fluids with temperatures ranging from 383 K to 823 K. ρ represents density, μ represents dynamic viscosity, k represents thermal conductivity, and Cp represents specific heat capacity at constant pressure. The solid region is made of 316L stainless steel, with a thermal conductivity of 16.3 W/mK.

Table 2: Thermo-physical properties of fluids

Fluid name	Polynomial function of the thermo-physical properties
Flue Gas	$\rho = 2.427 - 0.00608T + 6.54e\text{-}6T^2 - 2.56e\text{-}9T^3$, $\mu = 4.2e\text{-}6 + 5.05e\text{-}8T - 1.22e\text{-}11T^2$ $C_p = 1119.66 - 0.53T + 1.13e\text{-}3T^2 - 5.27e\text{-}7T^3$, $k = 0.00343 + 7.83e\text{-}5T - 1.43e\text{-}8T^2$
Dry Air	$\rho = 16.423 - 0.0402T + 4.23e\text{-}5T^2 - 1.62e\text{-}8T^3$, $\mu = 4.92e\text{-}6 + 5.064e\text{-}8T - 1.233e\text{-}11T^2$ $C_p = 1074.075 - 0.447T + 9.5e\text{-}4T^2 - 4.37e\text{-}7T^3$, $k = 0.00526 + 7.5584e\text{-}5T - 1.467e\text{-}8T^2$

2.3. Mathematical Model

The numerical simulations of the 3D counterflow heat exchanger are carried out using OpenFOAM, an open-source finite volume method (FVM) software. The energy, momentum, and continuity equations are solved in conjunction with the k-ω SST turbulence mode. The SIMPLE algorithm is applied for pressure-velocity field coupling. A solver called "chtMultiRegionSimpleFoam" is used from OpenFOAM. The second-order upwind schemes are used for energy and momentum, while first-order upwind schemes are used for turbulent kinetic energy and specific dissipation. The convergence criteria for all the residuals are less than 10^{-6}.

2.5. Parameter definitions

The geometrical parameters associated with an airfoil finned channel are fin length, fin thickness, fin height, transverse pitch, longitudinal pitch, and fin offset length. These parameters are illustrated in Fig. 1 and Table 1. Table 3 depicts the four geometrical parameters and their levels that are varied for parametric study to determine the effect on thermal-hydraulic performance. These parameters are expressed as dimensionless numbers with corresponding parameters except fin height. Fin length and fin thickness are not varied in this study.

The hydraulic diameter (D_h) on airside with airfoil fins is calculated by Eqs. (1-2) from a periodic element shown in Fig. 3.

$$D_h = \frac{4V_e}{A_{se}} \tag{1}$$

$$A_{se} = 2\left(P_a h_f/2\right) + 2\left(P_{fl}P_{ft} - S_a\right), \quad V_e = \left(P_{fl}P_{ft} - S_a\right)h_f \tag{2}$$

Here A_{se} and V_e represent the wetted surface area and the fluid volume of the periodic domain, respectively. P_a, and S_a represent the perimeter and cross-sectional area of the airfoil fin, respectively.

Table 3: Parameters formulae and levels of variation

Parameter name	Formula	Levels	Units
Height of airfoil	h_f	4, 6, 8, 10	mm
Transverse number	$\xi_t = P_{ft}/t_f$	2, 3, 4, 5	-
Longitudinal number	$\xi_l = P_{lf}/l_f$	2, 2.3, 2.6, 3	-
Offset number	$\xi_s = 2 \times (L_c/P_{fl})$	0, 0.33, 0.66, 1	-

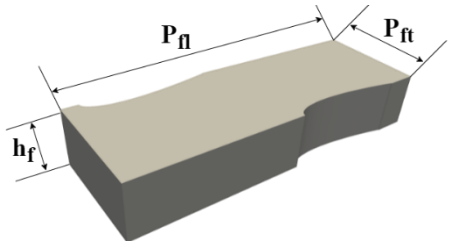

Fig. 3: Periodic domain

The thermal and hydraulic performance on the airside is evaluated using the Colburn-j factor and friction factor (f), respectively, calculated by Eqs. (3-4)

$$j = \frac{Nu_m}{RePr^{1/3}} \qquad Re = \frac{GD_h}{\mu} \qquad G = \frac{\dot{m}}{\phi A_{in}} \tag{3}$$

$$f = \frac{\Delta P}{2}\left(\frac{D_h}{L}\right)\frac{\rho}{G^2} \tag{4}$$

Here *Re* is the Reynolds number, *Pr* is the Prandtl number, Nu_m is the average Nusselt number, *G* is mass flux, and ϕ is porosity which is the ratio of fluid volume and total volume. All the thermo-physical properties in these formulae are calculated at mean temperature.

The inlet Reynolds number is calculated by Eq. (5)

$$Re_{inlet} = \frac{4\rho_{in}V_{in}A_{in}}{\mu_{in}P_{in}} \tag{5}$$

Here V_{in} is air velocity, A_{in} is cross-sectional area, P_{in} is perimeter, ρ_{in} is the air density, and μ_{in} is viscosity at the inlet section.

2.6. Mesh independence study and model validation

A grid independence test is necessary to confirm that the numerical solution will not be affected significantly due to changes in the mesh size or no. of cells. Figure 4 shows the heat exchanger's outlet temperature variation for both fluids. The graph shows that outlet temperature variation is insignificant after no. of cells = 1.2 x 10^7. So, the cell size corresponding to no. of cells = 1.2 x 10^7 is chosen as the optimal cell size for the remaining CFD studies.

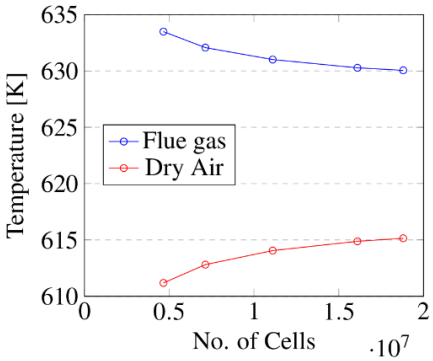

Fig. 4: Variation of outlet temperature

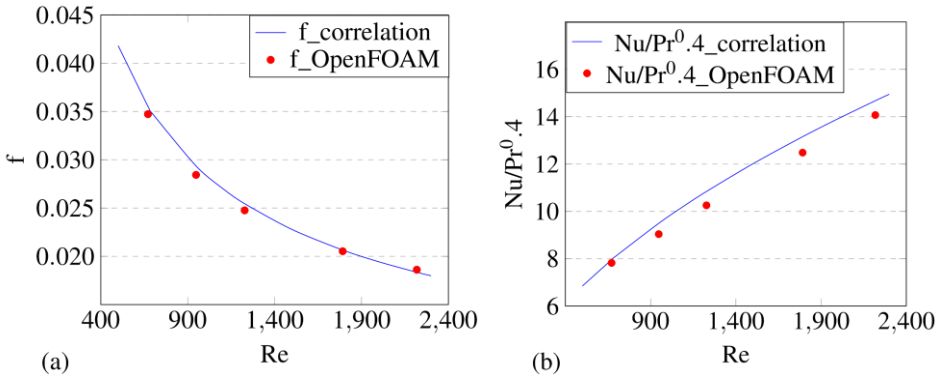

Fig. 5: Validation of (a) friction factor (b) Nusselt number

Validation of the numerical model is required to confirm the reliability of the simulation. Owing to the scarcity of data from experiments examining airflow in the airfoil channels, the numerical model is validated with numerical results from Chen et al. [10]. The validation results are presented in Fig. 5, comparing the present OpenFOAM simulated results and the correlation provided by Chen et al. [10]. The validation above shows that the numerical model utilized in this current work is suitable because the error for f and Nu is < 5 %.

3. Results and Discussions

In this section, the influence of geometrical parameters on thermal-hydraulic characteristics of airfoil fins on the airside is presented at Re_{inlet} of 1500 and discussed in detail.

3.1 Effect of Fin number

To determine the entrance effect, the number of fins or fin number effect on the thermal-hydraulic characteristics is investigated. The graphs are shown in Fig. 6(a) and Fig. 6(b), for a longitudinal number of 3, a transverse number of 5, a offset number of 1, and a fin height of 4 mm.

Due to the formation of a hydraulic boundary layer along the flow direction from the heat exchanger's inlet, the friction factor decreases from 2 to 25 fins at a decreasing rate, and after a certain point, it has to stabilise. But at fin number 25, the friction factor is not stabilized, but the variation from fin number 20-25 is 3.9 % only. The Colburn j-factor also decreases with the fin number due to the formation of a thermal boundary layer along the flow direction from the inlet of the heat exchanger, and beyond fin number 15, the boundary layer stabilizes, leading to a constant Colburn j-factor. Based on this study, a fin number of 20 is sufficient to analyze the thermal-hydraulic characteristics of an airfoil finned PFHE.

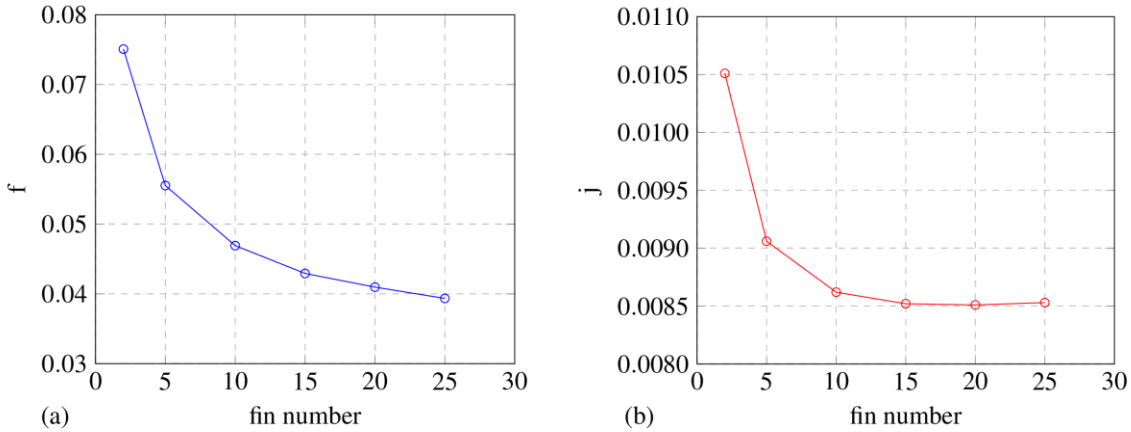

Fig. 6: (a) f vs. fin number (b) j vs. fin number

3.2 Effect of Offset Number (ξ_f)

Figure 7 and Fig. 8 show local cross-sectional area variation for a unit cell and the velocity distribution of air in the airfoil finned channel, respectively, for different offset number fins, which have a longitudinal number of 3, a transverse number of 5, and a fin height of 4 mm, As the offset number increases, the minimum flow cross-sectional area also increases, and the maximum flow velocity decreases, as seen from the velocity contour. For offset number = 0.66 and 1, the minimum cross-sectional area is the same, so the velocity contour looks similar for both cases.

Figure 9(a) and Fig. 9(b) show the variation of pressure drop per unit length ($\Delta P/L$) and heat transfer per unit area (Q/A) with offset number (ξ_f) and longitudinal number (ξ_l), respectively. For $\xi_l = 3$, the pressure per unit length and heat transfer per unit area decreases from $\xi_f = 0$ to $\xi_f = 0.66$ and becomes almost constant upto $\xi_f = 1$. This happens because $\xi_f = 0.66$ corresponds to $L_c = 4$ mm, which means the staggered moving fin is at the end of the fixed fin. From $L_c = 4$ mm, the minimum flow cross-sectional area is the same; hence the flow fields are similar with minor variations from $\xi_f = 0.66$ to 1. For $\xi_l = 2$, the pressure per unit length and heat transfer per unit area reduces, becoming minimum at $\xi_f = 1$, corresponding to $L_c = 4$ mm.

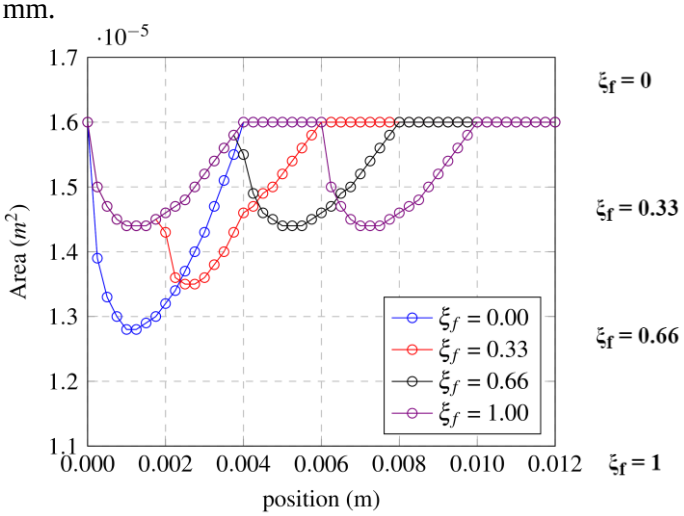

Fig. 7: Area Variation for $\xi_l = 3$

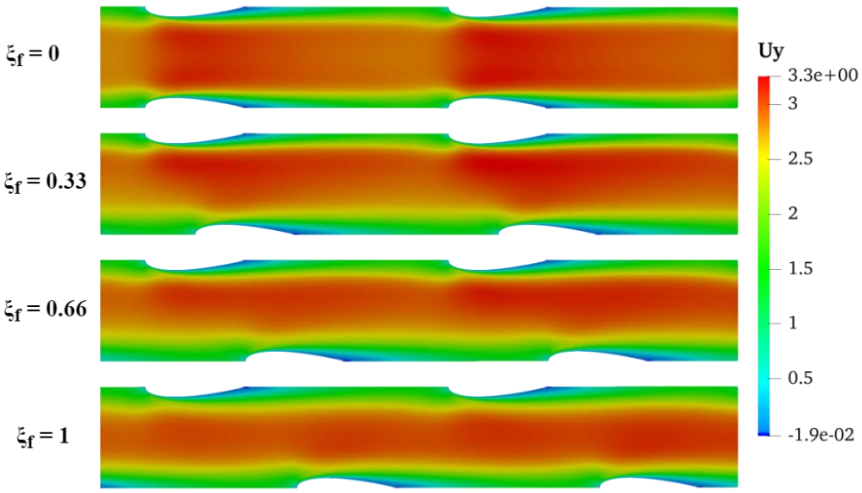

Fig. 8: Velocity contour for $\xi_l = 3$

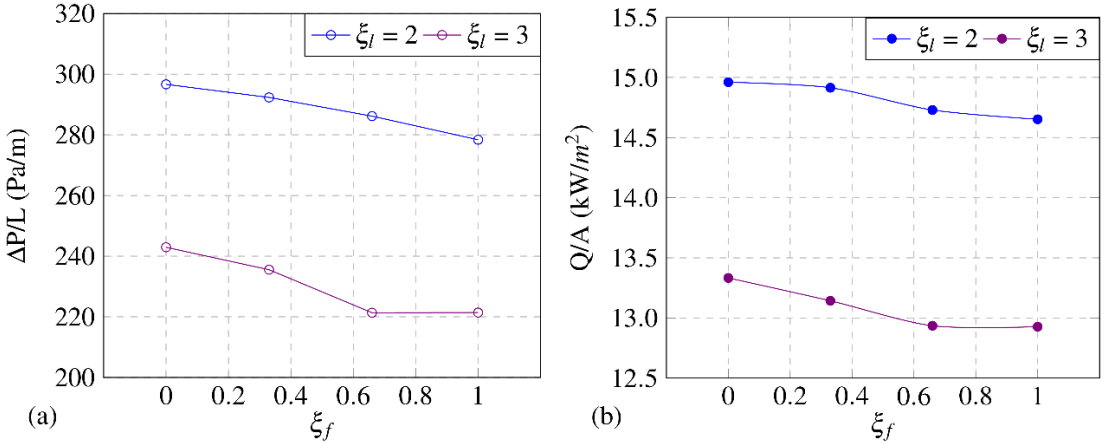

Fig. 9: Variation of (a) Pressure drop per unit length (b) Heat transfer per unit area with ξ_f and ξ_l

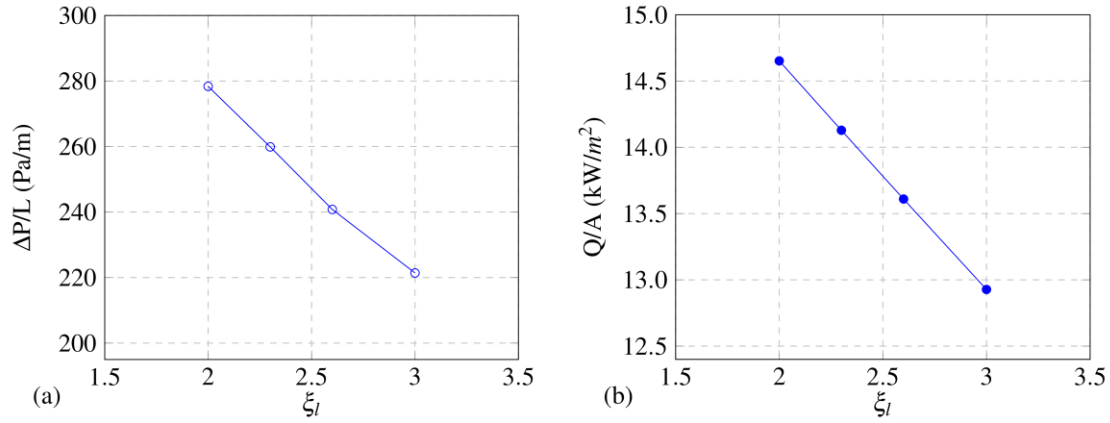

Fig. 10: (a) Pressure drop per unit length vs. ξ_l (b) Heat transfer per unit area vs. ξ_l

3.3 Effect of Longitudinal Number (ξ_l)

Figure 10 shows the variation of pressure drop per unit length and heat transfer per unit area for different longitudinal numbers, with a transverse number of 5, a offset number of 1, and a fin height of 4 mm.

Increasing the ξ_l increases the skin friction drag for a given number of fins because of the increased plate surface area. However, the decrease in fin density and fluid mixing results in less form drag, which offsets some of the increase in skin friction drag, resulting in a net decrease in pressure drop per unit length. The heat transfer coefficient on the plate surface is low compared to the heat transfer coefficient on the fin surface. The decrease in fin density also means less fin surface area is available for heat transfer, which leads to a decrease in the average heat transfer coefficient and a decrease in heat transfer per unit area.

3.4 Effect of Transverse Number (ξ_t)

Figure 11 shows the variation of pressure drop per unit length and heat transfer per unit area for different transverse numbers, which have a longitudinal number of 3, a offset number of 1, and a fin height of 4 mm.

For a given number of fins, increasing the ξ_t reduces the fin density and fluid mixing, resulting in less form drag. In addition, the flow velocities decrease with an increase in transverse number, leading to a reduced skin friction drag. As a result, the pressure drop per unit length decreases due to the reduction in form drag and skin friction drag. Although there is a reduction in average heat transfer coefficient due to lower local flow velocities and fin surface area, the decrease in heat transfer per unit area is not as significant as the decrease in pressure drop. As a result, the ratio of heat transfer per unit area to pressure drop per unit length is more at high transverse numbers.

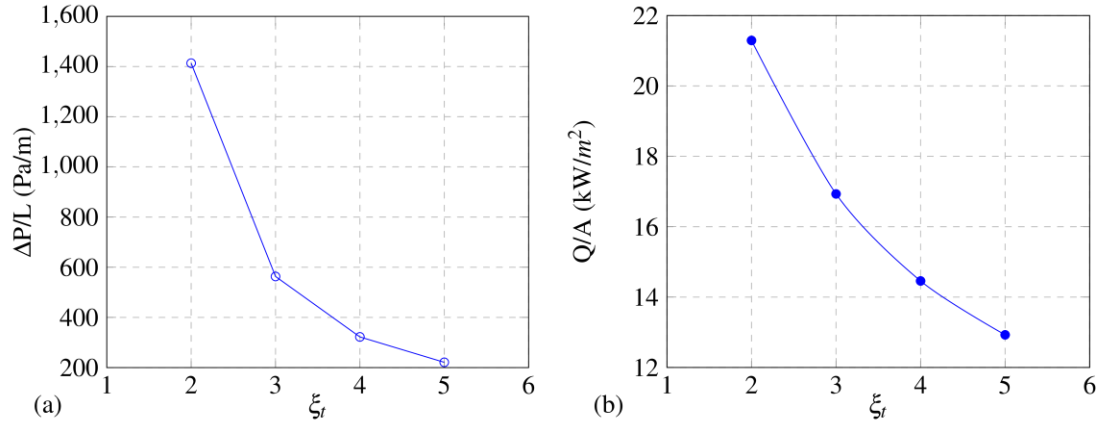

Fig. 11: (a) Pressure drop per unit length vs. ξ_t (b) Heat transfer per unit area vs. ξ_t

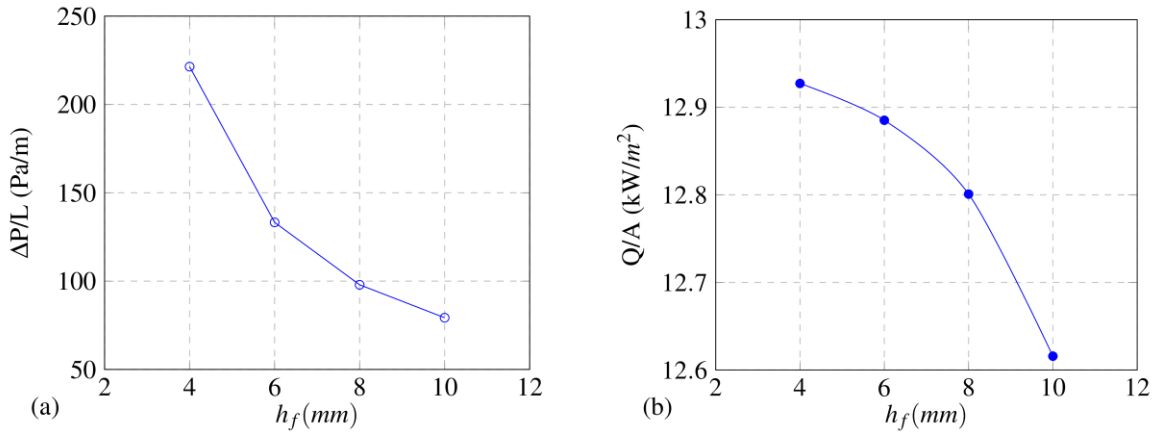

Fig. 12: (a) Pressure drop per unit length vs. h_f (b) Heat transfer per unit area vs. h_f

3.5 Effect of fin or channel height (h_f)

Figure 1212 displays the pressure drop per unit length and heat transfer per unit area for different fin heights, with a longitudinal number of 3, a transverse number of 5, and a offset number of 1.

As fin height increases, the non-dimensional flow velocities decrease, which reduces the skin friction drag and heat transfer coefficient. In addition, the form drag also decreases by the increase in fin height due to less flow velocities. As a result, the pressure drop per unit length and heat transfer per unit decreases. The rate of reduction in ΔP/L is faster, exhibiting a convex variation, and the rate of reduction in Q/A is slower, displaying a concave variation. As a result, the ratio of heat transfer per unit area to pressure drop per unit length is more at less channel or fin heights.

4. Conclusions

This current study adopted a heat exchanger unit structure of a waste heat recovery system, with dry air flowing inside an airfoil finned channel and flue gas flowing inside a straight channel. The effect of geometrical parameters on the thermal-hydraulic characteristics of dry air in the airfoil finned channel is investigated at Re_{inlet} = 1500. The following conclusions are drawn:

1. For different longitudinal numbers, the pressure drop per length and the heat transfer per unit area are maximum at ξ_f = 0, then decreases upto L_c = 4 mm and finally becomes constant upto offset distance corresponding to a completely staggered arrangement (ξ_f =1) for that particular longitudinal number.
2. As the longitudinal number, transverse number, and fin height increase, the pressure drop per unit length and heat transfer per unit area decrease. The change in longitudinal number linearly affects the ΔP/L and Q/A.
3. For transverse number (ξ_t) variation, both ΔP/L and Q/A exhibit convex non-linear variation. The overall thermal-hydraulic performance is more at a high transverse number.
4. For fin height (h_f) variation, ΔP/L exhibits convex non-linear variation, and Q/A shows concave non-linear variation. The overall thermal-hydraulic performance is more at less fin heights.

References

[1] W. M. Kays and A. L. London, *Compact heat exchangers*. 3d Ed., McGraw Hill: New York, 1984.

[2] R. K. Shah and D. P. Sekuli, *Fundamentals of Heat Exchanger Design*. John Wiley & Sons, 2007.

[3] S. Unger, M. Beyer, L. Szalinski, and U. Hampel, "Thermal and flow performance of tilted oval tubes with novel fin designs," *Int. J. Heat Mass Transf.*, vol. 153, p. 119621, 2020.

[4] S. Unger, M. Beyer, H. Pietruske, L. Szalinski, and U. Hampel, "Air-side heat transfer and flow characteristics of additively manufactured finned tubes in staggered arrangement," *Int. J. Therm. Sci.*, vol. 161, p. 106752, 2021.

[5] W. D. G. and D. Erno, "Introduction of an AM multi-furcating heat exchanger," *Proc. 16th IEEE Intersociety Conf.*

Thermal Thermomechanical Phenomena Electron. (ITherm), pp. 624-633, May 2017.
[6] M. Wong, I. Owen, C. J. Sutcliffe, and A. Puri, "Convective heat transfer and pressure losses across novel heat sinks fabricated by Selective Laser Melting," *Int. J. Heat Mass Transf.*, vol. 52, no. 1–2, pp. 281–288, 2009.
[7] S. Pracht, J. Will, S. Klöppel, T. Funke, H. Quack, and C. Haberstroh, "Experimental and numerical study of a 3D-printed aluminium cryogenic heat exchanger for compact Brayton refrigerators," *Cryogenics (Guildf).*, vol. 123, p. 103418, 2022.
[8] Z. X. Han, J. Guo, H. Zhang, J. Chen, X. Huai, and X. Cui, "Experimental and numerical studies on novel airfoil fins heat exchanger in flue gas heat recovery system," *Appl. Therm. Eng.*, vol. 192, p. 116939, 2021.
[9] H. Y. Shi, M. J. Li, W. Q. Wang, Y. Qiu, and W. Q. Tao, "Heat transfer and friction of molten salt and supercritical CO_2 flowing in an airfoil channel of a printed circuit heat exchanger," *Int. J. Heat Mass Transf.*, vol. 150, 2020.
[10] J. Chen, J. Guo, X. Li, X. Huai, K. Cheng, H. Zhang, Z. Han, "Thermal-hydraulic performance of compressed humid air flowing in a recuperator," *Appl. Therm. Eng.*, vol. 188, p. 116620, 2021.